Article

The Mechanism of Phagocytosis: Two Stages of Engulfment

David M. Richards[1,2,*] and Robert G. Endres[1,2]

[1]Department of Life Sciences and [2]Centre for Integrative Systems Biology and Bioinformatics, Imperial College, London, United Kingdom

ABSTRACT   Despite being of vital importance to the immune system, the mechanism by which cells engulf relatively large solid particles during phagocytosis is still poorly understood. From movies of neutrophil phagocytosis of polystyrene beads, we measure the fractional engulfment as a function of time and demonstrate that phagocytosis occurs in two distinct stages. During the first stage, engulfment is relatively slow and progressively slows down as phagocytosis proceeds. However, at approximately half-engulfment, the rate of engulfment increases dramatically, with complete engulfment attained soon afterwards. By studying simple mathematical models of phagocytosis, we suggest that the first stage is due to a passive mechanism, determined by receptor diffusion and capture, whereas the second stage is more actively controlled, perhaps with receptors being driven toward the site of engulfment. We then consider a more advanced model that includes signaling and captures both stages of engulfment. This model predicts that there is an optimum ligand density for quick engulfment. Further, we show how this model explains why nonspherical particles engulf quickest when presented tip-first. Our findings suggest that active regulation may be a later evolutionary innovation, allowing fast and robust engulfment even for large particles.

INTRODUCTION

Cells have evolved a whole host of mechanisms for ingesting particles and fluids. These vary from receptor-mediated endocytosis (absorption of small particles into clathrin-coated vesicles), to pinocytosis (the uptake of soluble material), to phagocytosis. Phagocytosis is the mechanism by which relatively large (>0.5 μm) particles, such as bacteria, dead cells, or (as here) polystyrene beads, are internalized (1–3). During phagocytosis in immune cells such as neutrophils and macrophages, receptors in the cell membrane first recognize antibodies on the target, which causes membrane protrusions called pseudopodia to surround the target in a zipperlike mechanism (see Fig. 1) (4,5). This is followed by fusion with lysosomes, acidification of the phagosome, and degradation of the target.

The most widely-studied example of phagocytosis involves Fcγ receptors, which recognize particles coated with immunoglobulin G (IgG) (6,7). Fcγ receptors are expressed in white blood cells in four different classes, distinguished by their antibody affinity (8). Upon binding to the Fc region of IgG, receptors signal via Syk kinases, small GTPases (9), and hundreds of other molecules, leading to substantial reorganization of the actin cytoskeleton and its contraction by multiple myosin isoforms (10,11). The resulting complexity (12) has the potential to obscure the fundamental processes and principles that, as often is the case in biology, may well be quite simple. In particular, the connection between fundamental physical mechanisms

and biological regulation remains to be explained. Focusing on only the most important components, such as the receptors, ligand density, and particle shape, may help elucidate the fundamental underlying mechanisms of engulfment.

Despite phagocytosis being discovered more than 100 years ago (13), there are relatively few theoretical models of cup formation and receptor dynamics. In Herant et al. (14,15), finite-element computations were used to argue that engulfment requires two crucial interactions: 1), repulsion at the cup edge between the membrane and newly-polymerized actin; and 2), a flattening force within the cup. Conversely, van Zon et al. (16) modeled the motion of receptors and F-actin in an attempt to explain the fact that phagocytosis normally either fully completes or stalls before half-engulfment. In Tollis et al. (17), zipper-like engulfment was modeled as an actin-driven ratchet mechanism, leading to robust engulfment. However, none of these models allow for different physical and biological mechanisms to operate at different stages of engulfment.

In addition to these phagocytosis models, there is an elegant approach to modeling the related problem of endocytosis (18). This model maps the motion of receptors within the membrane to the well-known Stefan problem; in fact, to the supercooled Stefan problem. The Stefan problem, introduced in the nineteenth century, applies to first-order phase transitions governed by the heat equation. The archetypal example is that of the melting of ice, where the boundary between water and ice continually moves as more ice melts. This is remarkably similar to the cup
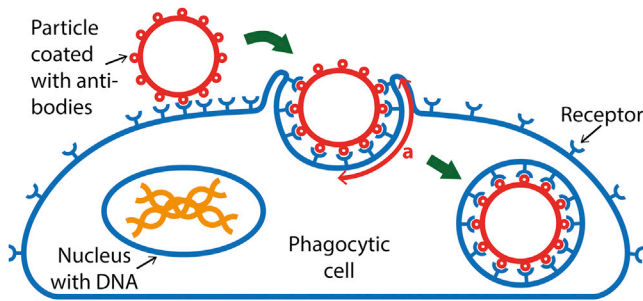

FIGURE 1 Phagocytosis of a target particle. Receptors on the cell surface bind ligand molecules on the target, such as a pathogen, dead cell, or bead. As receptors bind more and more ligand molecules, the cell membrane progressively engulfs the target. Upon full engulfment, a phagosome is formed, which fuses with lysosomes, leading to digestion of the target. We denote the arc length of engulfed membrane by a, which gradually increases during engulfment. To see this figure in color, go online.

boundary during engulfment, which increases as receptors flow toward the cup, now determined by the diffusion equation. Using this correspondence, it was shown that there exists an optimum particle size during endocytosis corresponding to the shortest engulfment time: particles both larger and smaller than this optimum size take longer to engulf. Although phagocytosis is considered a more active, more regulated process than endocytosis, it is quite possible that early events in phagocytosis are driven by passive processes and may share similarities with endocytosis.

In this article, we focus on the progression of engulfment, in particular on the rate of engulfment and its dependence on passive and active mechanisms. For a spherical bead with radius R, we define the engulfment, a, as the arc length from the center of the cup to the edge of the cup. At the start of phagocytosis, $a = 0$, with a then monotonically increasing during engulfment, reaching πR upon full engulfment (see Fig. 1). Naively, one might expect that a initially increases quickly (because membrane wrinkles are used to extend the membrane around the particle), followed by a slower stage as new membrane must be synthesized or brought from internal stores (19,20). Interestingly, we will find exactly the opposite. By analyzing multiple single-bead, single-cell movies, we find evidence for two distinct stages of engulfment: an initial slow stage followed by a much quicker second stage.

We then extend the passive endocytosis model of Gao et al. (18) to describe phagocytosis of spherical beads. Because phagocytosis of large particles is considered more active (for example, more actin-dependent) than endocytosis, we then expand this model to include processes such as receptor drift and signaling, finding good agreement with the experimental data. We then examine the effect of ligand density on the engulfment time, predicting that particles with intermediate density are engulfed quickest. Finally, we study how ellipsoidal particles are engulfed,

providing a potential explanation for why such particles are more likely to be engulfed when the highly-curved tip is presented to the cell first.

MATERIALS AND METHODS

Phagocytosis movies

We studied six movies, four using 4.6-μm-diameter beads and two using 6.2-μm-diameter beads. Briefly, polystyrene beads were incubated first in BSA (bovine serum albumin) and then with rabbit anti-BSA antibody. Human neutrophils and beads were then picked up in separate micropipettes and brought into contact. Upon adhesion, the bead was released and phagocytosis observed under a bright-field microscope using a 63× objective. The aspiration pressure was continually adjusted to ensure the length of cell within the micropipette was constant. Because only a small part of the cell is within the pipette, we believe that this continual pressure adjustment is unlikely to effect phagocytosis. This is confirmed by previous work that uses the same setup (14,21,22). For details, see Herant et al. (23).

Image analysis

For each frame of a movie, the cell, bead, and pipette were automatically identified. Initially edge detection, using the Sobel method, was performed, after which the bead was found by using a Hough transform. This identified the center and radius of the bead in each frame. The pipette was identified by searching for a set of horizontal lines, capped by a vertical line (as in Fig. 2 B). Due to the phagocytic cup, the cell is not well described by a sphere. However, it was still possible to find the body of the cell (the cell minus the cup) by assuming the body was spherical. After removing the bead, pipette, and cell body from each frame, all that remained is the phagocytic cup, which was separated from the background by imposing a threshold. Finally we measured the size of the phagocytic cup, defined as the arc length of bead circumference bound to the cell membrane. For full details, see the Supporting Material.

Data fitting

We scanned through a discretized version of parameter space that was described by

$$A_1, A_2 = \{0.05, \ 0.1, \ 0.15, \dots, \ 5.0\},$$

$$\alpha_1, \alpha_2 = \{0.05, \ 0.1, \ 0.15, \dots, \ 1.5\},$$

$$t_0, t_1 = \{0, \ 1, \ 2, \dots, \ T\},$$

where T is the total length of the movie and $t_0 < t_1$. For each point in this space, we define the error as

$$\sum_i (a_i - \overline{a}_i)^2,$$

where a_i is the measured engulfment from frame i, $\overline{a}_i$ is given by Eq. 1 applied at $t = t_i$, and the sum runs over all frames. The minimum error gives the best fit to the measured data. To test that the difference between the α_1 and α_2 distributions is statistically significant, we used the Mann-Whitney U-test, a nonparametric test often used for nonnormally distributed data, finding significance with $p < 0.02$ ($U = 107.5$, $n_{\alpha_1} = n_{\alpha_2} = 12$).
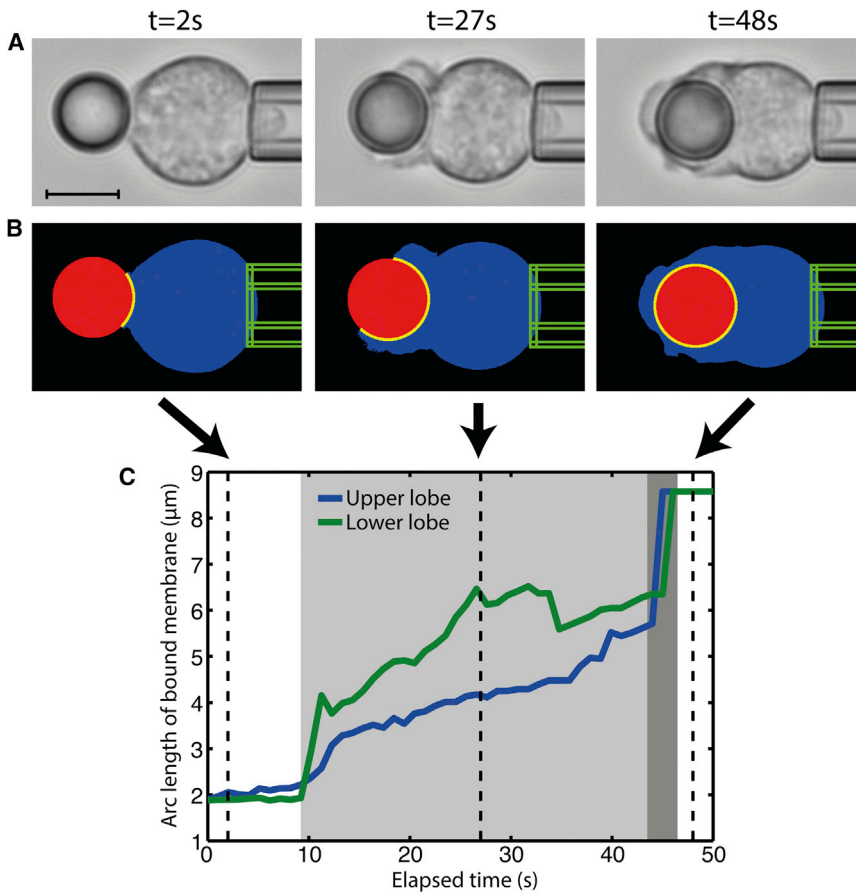
FIGURE 2 Typical time-lapse movie and image analysis of neutrophil engulfing an IgG-coated bead. Here the bead has diameter 4.6 μm. Data from Herant et al. (14). (A) Raw images of three frames at various stages of engulfment. At t $\approx$ 2 s, the bead has been released onto the cell, with a contact area of a $\approx$ 2 μm. At this point engulfment has not yet started. At t $\approx$ 27 s, the bead is approximately half-engulfed, with the lower lobe noticeably ahead of the upper lobe. At t $\approx$ 48 s, engulfment is complete, the bead is entirely within the cell, and the phagosome is fully formed. Scale bar: 5 μm. (B) The same frames as in panel A after automatic image analysis. (Blue) Cell; (red) bead; (green) outline of the pipette; (yellow) membrane attached to the bead. (C) Engulfment as a function of time. For both the upper and lower lobes, after engulfment begins at t $\approx$ 10 s, there is an initial slow stage (light gray) followed by a much quicker second stage (dark gray). Engulfment is complete by t $\approx$ 46 s. To see this figure in color, go online.

Numerical simulations

The diffusion-and-drift model and the model with signaling were solved numerically as follows. The membrane was represented by a finite grid of length $L = 50$ μm and spacing $\Delta r = 0.01$ μm, labeled by i. Given the values of $\rho_i(t)$, $S_i(t)$, and $a(t)$ at some time t, the values at the next time step, $t + \Delta t$ ($\Delta t = 2.5 \times 10^{-5}$ s), were found from the Euler method and by imposing the boundary condition $\rho_{i(a)}(t + \Delta t) = \rho_+$, where $i(a)$ is a expressed as an integer number of lattice steps and ρ_+ is found by solving Eq. 4. As a check of the numerical method and to ensure that values of Δr and Δt were sufficiently small, we checked that the numerical and analytic solutions matched for the pure diffusion and pure drift models. We also checked that decreasing Δr and Δt did not noticeably change the results, indicating convergence. See the Supporting Material for full details.

Parameter values

Parameter values were chosen as follows:

- $D = 1$ μm^2 s^{-1}, close to the Fcγ receptor diffusion constant reported in van Zon et al. (16);
- $v = 0.1$ μm s^{-1}, chosen so that engulfment after 1 min is similar in the pure diffusion and pure drift models;
- $\rho_0 = 50$ μm^{-2}, typical receptor density (18,24);
- $\rho_L = 500$ μm^{-2}, typical ligand density (25);
- $\varepsilon = 15$, measured FcγR-IgG binding free energy (15 $k_B T$) (26);
- $\beta = 20$, typical value of bending modulus (20 $k_B T$) (27);
- $R = 2$ μm, similar radius to the beads in our data; and
- $L = 50$ μm, approximate circumference of our cells.

RESULTS

Phagocytosis proceeds in two stages

We analyzed six time-lapse movies of FcγR-mediated neutrophil phagocytosis, four with beads of 4.6-μm diameter and two with beads of 6.2-μm diameter (one of which is published in Herant et al. (14)). Example frames are shown in Fig. 2 A. These were obtained by holding IgG-coated beads and neutrophils in separate micropipettes, before bead and cell were brought into contact and released. Image analysis was performed automatically to remove any human bias. Briefly, we used a combination of edge detection and Hough transforms to identify the position and size of the cell, bead, and pipette. After removing the bead, a threshold was applied, allowing the shape of the membrane engulfing the bead to be identified, from which the arc length of membrane engulfing the cell was calculated. For full details, see Materials and Methods. Examples of this analysis are shown in Fig. 2 B; see also Movie S1 in the Supporting Material.

In our focal plane we can identify two lobes of the phagocytic cup, which we refer to as the top and bottom (Fig. 2 A). Although the top and bottom lobes are connected, we analyzed them separately. Fig. 2 C shows a typical result of the engulfed arc length as a function of

time, with the remaining plots shown in Fig. S1 in the Supporting Material. Initially, there is a period (0–10 s in Fig. 2 C) when the bead is in contact with the cell, although engulfment has not started. This results in a nonzero, approximately constant contact length between the bead and cell, due to adhesion between them. At some point (~10 s in Fig. 2 C), engulfment begins and the engulfed arc length starts to increase as a function of time. Initially, this engulfment is relatively slow, with the rate of further engulfment decreasing in time. However, at some point (~44 s in Fig. 2 C) there is a sharp and rapid increase in engulfment rate, with full engulfment occurring soon after (~46 s in Fig. 2 C). These two stages of engulfment, an initial slow stage followed by a rapid second stage, occurred for both 4.6- and 6.2-μm beads. Surprisingly, engulfment in the slow stage proceeds at different rates in the top and bottom lobes. This suggests that, at least initially, engulfment is a local process, depending only on the distribution of receptors at a given point on the membrane.

Power laws describe engulfment

To test the idea of two distinct stages, we fit our data to a general two-step model by assuming that each stage is described by an independent power law. To this end, we describe the engulfed arc length, $a(t)$, in four parts (Fig. 3 A):

1. After the bead initially makes contact with the cell, there is a time when the bead sits on the surface of cell, with some nonzero engulfment, a_0.
2. After some time t_0, engulfment begins and the first, slower stage starts. We describe this using a power law, $a(t) \sim A_1 t^{\alpha_1}$, shifted so that $a = a_0$ at $t = t_0$.
3. At time t_1 when the engulfment is a_1, the second, faster stage is initiated, described by an independent power law, $a(t) \sim A_2 t^{\alpha_2}$, this time shifted so that $a = a_1$ at $t = t_1$.
4. At time t_2, the bead is completely engulfed and the engulfed arc length reaches its maximum of a_2.

Thus we model the engulfed arc length, where $a_1 = a_0 + A_1(t_1 - t_0)^{\alpha_1}$ and $a_2 = a_1 + A_2(t_2 - t_1)^{\alpha_2}$, as

$$a(t) = \begin{cases} a_0 & \text{for } t < t_0, \\ a_0 + A_1(t - t_0)^{\alpha_1} & \text{for } t_0 \leq t < t_1, \\ a_1 + A_2(t - t_1)^{\alpha_2} & \text{for } t_1 \leq t < t_2, \\ a_2 & \text{for } t \geq t_2. \end{cases} \quad (1)$$

We observed that a_0, the initial contact between the bead and cell, is approximately constant in all our movies, even for different bead sizes, with an average and standard deviation of $a_0 = 2.10 \pm 0.20$ μm. Thus, to reduce the number of parameters in the general model, we set $a_0 = 2.10$ μm from now on. Further, a_2, the arc length of membrane wrapping the bead at full engulfment, can readily be determined by examining the final few frames of each movie, after engulfment is complete. Thus, for any given movie, there are only six parameters to fit: the times t_0, t_1, the powers α_1, α_2, and the prefactors A_1, A_2 (see Materials and Methods for details).

The change from the slow to fast stage of engulfment occurs when the average fraction of bead engulfed is 0.47 ± 0.10, suggesting that the fast stage may be triggered at approximately half-engulfment when further engulfment requires the purse-string-like closure of the membrane around the bead (28). To examine the relative speeds of the first and second stages, we consider the fraction of total engulfment time spent in the first stage compared to that in the second, finding an average of 0.77 ± 0.15. This means that, on average, the first stage lasts more than three times longer than the second stage, despite the fact that both stages engulf approximately half the total bead area. In addition to this, the parameters α_1 and α_2 give information about the exact manner in which engulfment proceeds during each stage. We find that the median of α_1 is 0.68 whereas that of α_2 is 1.0 (see Fig. 3 B for medians and upper and lower quartiles), suggesting that the stages may be governed by entirely different processes.

We can also examine whether there are differences in engulfment between our two bead sizes. For the average total engulfment time, $t_2 - t_0$, we find, as expected, that
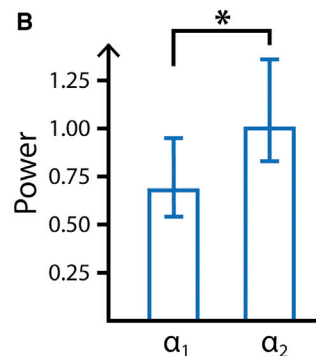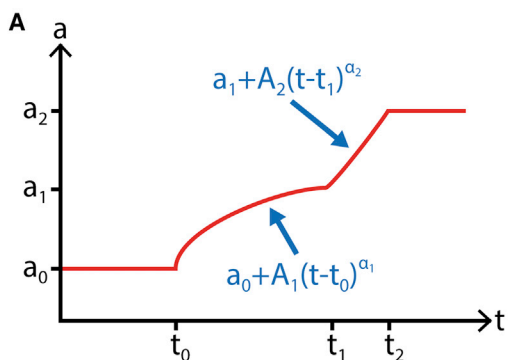

FIGURE 3 Fitting to the general model. (A) The general two-stage model is split into four regions. First, before engulfment begins, the contact length is constant with $a = a_0$. Second, after engulfment begins at $t = t_0$, the engulfed arc length is given as a power law with power α_1 and prefactor A_1. Third, after $t = t_1$, the second step begins and a is described by an independent power law with power α_2 and prefactor A_2. Fourth, after $t = t_2$, the particle is completely engulfed and $a = a_2$. (B) Comparison of the two powers, α_1 and α_2, showing the median and upper and lower quartiles. $n_{\alpha_1} = n_{\alpha_2} = 12$ (6 beads × 2 lobes). A Mann-Whitney U-test showed that the difference between α_1 and α_2 is significant ($p < 0.02$, $U = 107.5$). To see this figure in color, go online.

the larger beads take longer to engulf (37 $\pm$ 8 s for 4.6-μm beads and 90 $\pm$ 12 s for 6.2-μm beads). This relatively large increase is probably due to the available membrane becoming limiting for 6.2-μm beads, when the bead radius becomes similar to the cell radius. However, the fraction of bead engulfed at the start of the second stage is similar for both bead sizes (0.49 for 4.6-μm beads and 0.44 for 6.2-μm beads). Our data is insufficient to determine whether this small difference is significant. Finally, the change in α between the stages is again consistent for both radii (0.63 $\rightarrow$ 1.0 for 4.6-μm beads and 0.83 $\rightarrow$ 1.1 for 6.20-μm beads), suggesting that the two-stage mechanism is a general feature of phagocytosis, independent of bead size.

Pure diffusion model

To try to understand the possible origins of such different dynamics, we consider simple models, focusing mainly on the motion of the Fcγ receptors. Motivated by Gao et al. (18), we consider a circularly-symmetric two-dimensional membrane, with the origin being the point at which the bead first touches the cell. This is a reasonable assumption, given the spherical symmetry of the bead. The model describes aspects both of endocytosis (18) and of CR3-mediated phagocytosis where the bead normally sinks into the cell, as in Fig. 4 A. Even in Fcγ-mediated phagocytosis, where engulfment is by extension of the membrane around the bead (Fig. 4 B), the problem is still one of receptors moving in a two-dimensional membrane. Because in our simple model we neglect the details of the cup shape, the only relevant difference is that the total curvature is greater in the Fcγ-mediated case (although the local curvature is approximately the same, a greater area of membrane is curved). Thus, by including this extra curvature, we can also apply the same model to Fcγ-mediated phagocytosis (see the Supporting Material for details).

Due to the assumed circular symmetry, the problem reduces to receptors moving on a semi-infinite one-dimensional line. We parameterize this line by the distance from the origin, r, and describe the receptor density by $\rho(r,t)$, where t is the time. Before contact with any bead, the receptor density is independent of r and is given by ρ_0. During engulfment, the receptor distribution is no longer constant, although the density at infinity is always ρ_0. The second variable is the cup size, $a(t)$, the engulfed arc length measured from the center of the cup. Within the engulfed region, where $r < a$, receptors are attached to the ligands on the bead. As such, their density is assumed to be related to the ligand density on the bead and, for simplicity, we assume that ρ in this region is constant and given by ρ_L, where $\rho_L > \rho_0$. We denote the receptor density at the cup edge, $\rho(a(t),t)$, by $\rho_+(t)$. These variables and constants are shown in Fig. 4 C.

There are various possible physical mechanisms for the motion of the receptors in the nonengulfed region of the
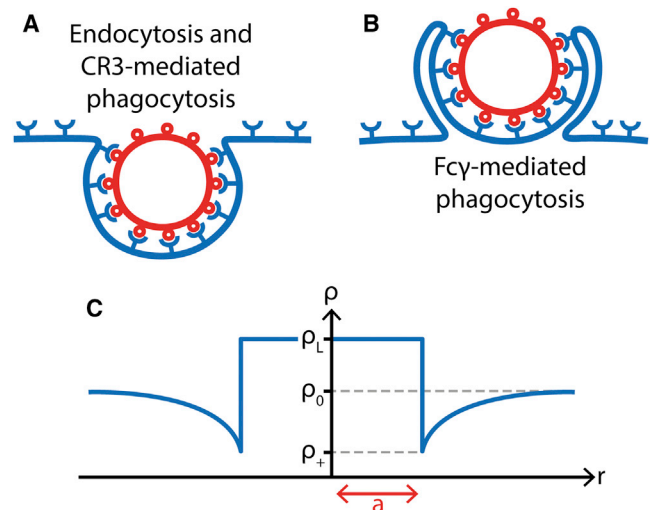

FIGURE 4 Types of phagocytosis and the model variables. (A) In CR3-mediated phagocytosis, the particle sinks into the cell, in a manner similar to endocytosis. (B) In contrast, in Fcγ-mediated phagocytosis, the membrane extends via pseudopod extensions outwards around the particle. Despite these differences, we believe that the movement of receptors within the membrane is similar in both cases, and can be described by the same simple model. (C) Sketch of the receptor density, ρ, which depends only on the distance from the center of the cup, r, and the time, t. Within the cup, which has arc length a, the receptor density is always fixed at ρ_L, whereas the density at infinity, which is the same as the initial density, is ρ_0. At the edge of the cup, the receptor density is fixed at ρ_+, which is calculated by considering the free energy. In the pure diffusion model, ρ_+ is always less than ρ_0, so that receptors always flow in toward the cup and increase the cup size. To see this figure in color, go online.

membrane, $r \geq a$. The first we consider is a purely passive process, where receptors simply diffuse around the membrane (18). Diffusion of ρ is then described by $\partial\rho/\partial t = D\nabla^2\rho$, where ∇^2 is the radial part of the Laplacian in cylindrical coordinates and D is the diffusion constant. The evolution of a is determined by conservation of receptors. Receptors move from outside to inside the cup region with flux $-D\rho'_+$, where ρ'_+ is shorthand for $\partial\rho/\partial r$, evaluated at $r = a$. This flux increases the density of receptors in the boundary region from ρ_+ to ρ_L, from which the rate of change of a follows. See the Supporting Material for details. Thus, our pure diffusion model, for the nonengulfed region of the membrane (where $r \geq a$), which is identical to the (supercooled) one-dimensional Stefan problem, is described by

$$\frac{\partial\rho}{\partial t} = \frac{D}{r}\frac{\partial}{\partial r}\left(r\frac{\partial\rho}{\partial r}\right), \tag{2a}$$

$$\frac{da}{dt} = \frac{D\rho'_+}{\rho_L - \rho_+}, \tag{2b}$$

with initial conditions $\rho(r,0) = \rho_0$ and $a(0) = 0$.

To find a solution to this system, one extra condition is needed. Following Gao et al. (18), we require that there is

no free-energy change as receptors move into the engulfed region and the cup boundary is extended, indicating that all energy from receptor-ligand binding and configurational receptor entropy is used for bending the membrane and engulfment. We consider three contributions to the free energy: 1), the binding between receptors and ligands, 2), the curvature of the membrane, and 3), the receptor entropy. The negative energy from binding is necessary to cancel the positive contribution from membrane curvature. As explained in the Supporting Material, we can write the free energy, $\mathscr{F}$, as

$$\frac{\mathscr{F}}{2\pi k_B T} = \int_0^a \left(-\rho_L \mathscr{E} + \frac{1}{2}\mathscr{B}\kappa_p^2 \right) r dr + \int_0^\infty \rho \ln\left(\frac{\rho}{\rho_0}\right) r dr, \tag{3}$$

where $\mathscr{E}$ is the binding energy per receptor-ligand bond, $\mathscr{B}$ is the bending modulus, and κ_p is the radius of curvature of the bead. Although we do not explicitly include the membrane tension, such a term could be absorbed into the definition of $\mathscr{E}$ (see the Supporting Material). For a spherical bead of radius R, $\kappa_p = 2/R$. Requiring no free-energy jump across the cup boundary implies that

$$\frac{\rho_+}{\rho_L} - \ln\left(\frac{\rho_+}{\rho_L}\right) = \mathscr{E} - \frac{\mathscr{B}\kappa_p^2}{2\rho_L} + 1, \tag{4}$$

from which it follows that ρ_+, the receptor density at the cup edge, is a constant, independent of time. The (numerical) solution for ρ_+ gives the extra condition needed to uniquely solve the system (Eq. 2).

The solution, shown in Fig. 5 A, is then given by

$$\rho(r,t) = \begin{cases} \rho_L & \text{for } r<a, \\ \rho_0 - AE_1\left(\frac{r^2}{4Dt}\right) & \text{for } r \geq a, \end{cases} \tag{5a}$$

$$a(t) = 2\alpha\sqrt{Dt}, \tag{5b}$$

where

$$E_1(x) = \int_x^\infty \frac{e^{-u}}{u} du$$

is the exponential integral. As explained in the Supporting Material, the constant α is found by solving (numerically)

$$\alpha^2 e^{\alpha^2} E_1(\alpha^2) = \frac{\rho_0 - \rho_+}{\rho_L - \rho_+}, \tag{6}$$

after which A is given by $A = (\rho_0 - \rho_+)/E_1(\alpha^2)$. The most important property of the solution is the behavior of a, which increases as the square-root of time, $a \propto \sqrt{t}$. This is similar to the behavior we found when fitting the first stage of our movie data to the general model, suggesting that the first stage is controlled by passive receptor diffusion and capture.
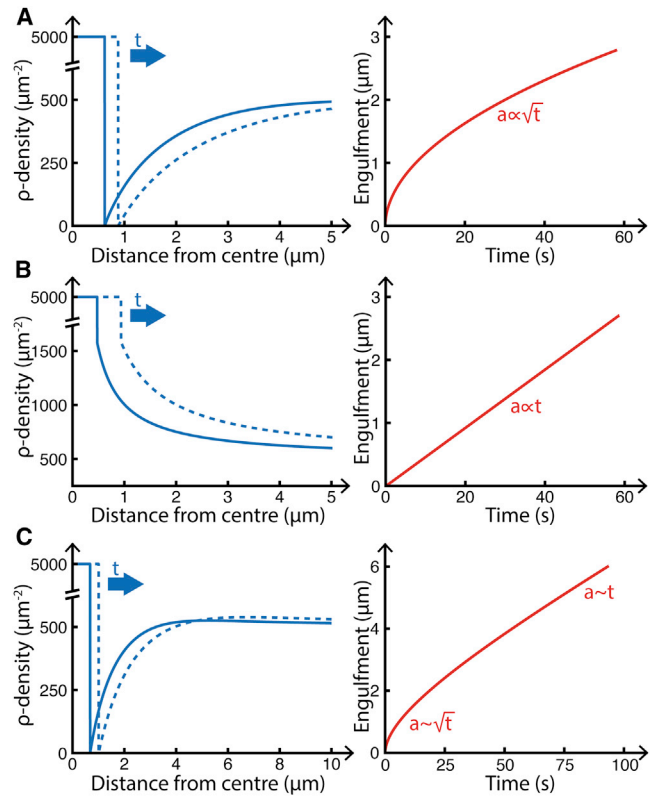

FIGURE 5 Results from the pure diffusion, pure drift, and diffusion-and-drift models. (Left) Receptor density profile. (Right) Engulfment against time. (A) Pure diffusion model with $D = 1$ μm^2 s^{-1}. The receptor density, ρ, drops significantly just outside the cup so that $\rho_+ < \rho_0$ and evolves to the right as engulfment proceeds. Note that the parameters are such that $\rho_+ \approx 0$. The engulfment increases as the square-root of time. Receptor profile shown at $t = 3$ s (solid) and $t = 6$ s (dashed). (B) Pure drift model with $v = 0.1$ μm s^{-1}. The receptor density has a completely different profile and decreases away from the cup, with ρ_+ now greater than ρ_0. Importantly, the engulfment now increases linearly in time. Receptor profile shown at $t = 10$ s (solid) and $t = 20$ s (dashed). (C) Diffusion and drift model with $D = 1$ μm^2 s^{-1} and $v = 0.1$ μm s^{-1}. Engulfment now proceeds as a mixture of the pure diffusion and pure drift cases. Initially, when the receptor density is low, $a \sim \sqrt{t}$ as in the pure diffusion model. At later times, when the receptor gradient near the cup becomes approximately constant, a becomes more linear in time and behaves more like the pure drift result. Receptor profile shown at $t = 3$ s (solid) and $t = 6$ s (dashed). Parameters are $\rho_0 = 50$ μm^{-2}, $\rho_L = 5000$ μm^{-2}, $\mathscr{E} = 15$, $\mathscr{B} = 20$, $R = 2$ μm, and $L = 50$ μm. To see this figure in color, go online.

Pure drift model

In contrast to this purely diffusive, passive model, we now consider the other extreme: a model where receptors are actively moved toward the edge of the cup. To do this, we remove any diffusion and instead impose that the receptors drift with constant velocity toward the boundary $r = a$, requiring some active centripetal force, such as movement of receptors via retrograde actin flow (29). The movement of the receptors is now described by $\partial\rho/\partial t = v\nabla \cdot \rho$, where $\nabla \cdot$ only includes the radial part of the divergence in cylindrical coordinates and v is the drift velocity. The equation

for a is also changed because now the flux across the cup boundary is $-v\rho_+$. Thus, our second model (which is also a type of Stefan problem, but with diffusion replaced by drift) is given by

$$\frac{\partial \rho}{\partial t} = \frac{v}{r} \frac{\partial}{\partial r} (r\rho), \tag{7a}$$

$$\frac{da}{dt} = \frac{v\rho_+}{\rho_L - \rho_+}, \tag{7b}$$

with the same initial conditions as before.

Unlike for the diffusion model, there is no need for the extra condition obtained from free-energy considerations. The analytic solution, shown in Fig. 5 B, is given by

$$\rho(r,t) = \begin{cases} \rho_L & \text{for } r < a, \\ \rho_0 \left(1 + \frac{vt}{r}\right) & \text{for } r \geq a, \end{cases} \tag{8a}$$

$$a(t) = \frac{1}{\sqrt{\rho_L/\rho_0} - 1} vt. \tag{8b}$$

The receptor density at the edge is given by

$$\rho_+ = \sqrt{\rho_L \rho_0},$$

which means that, because Eq. 4 will not in general be satisfied, it is impossible to avoid a free-energy jump across the boundary in this model. In contrast to the diffusion model, the rate of engulfment is now linear in time, $a \propto t$, which suggests that the drift model is more appropriate for the second, faster stage of engulfment, where, on average, we found $\alpha_2 = 1.0$.

Combining diffusion and drift

The pure diffusion and pure drift models are extreme cases, where the receptors either diffuse or drift, but not both. It is far more realistic to allow both behaviors, which results in a system that looks like a combination of Eqs. 2 and 7. As for the pure diffusion model, we again consider the free energy and require that there is no energy jump across the cup. Despite the addition of drift, the resulting equation for ρ_+ is unchanged from Eq. 4, so that the receptor density at the cup is again constant, independent of time. See the Supporting Material for details.

Unlike the pure diffusion and pure drift cases, this model cannot be solved analytically. Instead, as explained in Materials and Methods, we numerically solved the system on a finite-grid membrane. An example of the output is shown in Fig. 5 C. Near the cup, the receptor profile looks similar to the pure diffusion case, with positive gradient so that diffusion (in addition to drift) causes receptors to flow across the boundary and increase the cup size. Further from the cup, the density increases beyond the value at infin-

ity, ρ_0, before turning around and decreasing back toward ρ_0. As with the pure diffusion model, the engulfed arc length $a(t)$ initially grows as $\sqrt{t}$. This is because, at early times, the flow of receptors into the cup is dominated by the relatively large gradient of ρ. At later times, when $\partial\rho/\partial r$ decreases, drift is the dominant cause of receptor flow, and $a(t)$ grows linearly with time. Thus, the combined diffusion and drift model initially looks like pure diffusion, with later behavior more similar to pure drift.

A full model that captures both phases of engulfment

Although the diffusion and drift model displays $a \sim \sqrt{t}$ and $a \sim t$ regimes, it is clear that it cannot explain the sharp jump in Fig. 2 C. To progress further, we consider, in addition to the receptors, the role of signaling via a signaling molecule described by density S. Although phagocytosis in a real cell depends on many types of signaling molecules in complicated cascades, it is not unreasonable to assume that just one species will capture the essential manner in which signaling influences the receptor dynamics. For simplicity, we imagine that our signaling molecule only moves within the membrane, as happens for some small GTPases. Due to the circular symmetry of the system, the signaling molecule, as with the receptors, can be described as a function of the distance from the origin r and the time t, so that $S = S(r,t)$.

We assume that initially there are no signaling molecules and that S is produced with constant rate in response to receptor-ligand binding. As such, S is only produced within the cup region where $r < a$. To counteract the production, we also allow S to degrade everywhere with constant lifetime. Finally, we let S diffuse throughout the membrane with diffusion constant D_S, which is generically different to the receptor diffusion constant D. Thus the dynamics of S (as sketched in Fig. 6 A) are described by

$$\frac{\partial S}{\partial t} = \frac{D_S}{r} \frac{\partial}{\partial r} \left(r \frac{\partial S}{\partial r}\right) + \beta\rho_L \Theta(a - r) - \tau^{-1} S, \tag{9}$$

where $\Theta(x)$ is the Heaviside function, $\beta\rho_L$ is the binding rate, and τ is the lifetime. For full details, see the Supporting Material.

In order that the signaling molecule can influence engulfment, i.e., that S can actually signal, we need to couple S to the dynamics of ρ. There are several ways we could do this, although we focus on the case where the density of the signaling molecule influences the drift speed. This can lead to radically different types of engulfment. For example, if we assume $v = v_1 S$ for some constant v_1, it is possible to get accelerated cup growth as shown in Fig. 6 B. In such a model there is initially no signaling, and therefore no drift. However, as the signaling molecule density at the cup edge
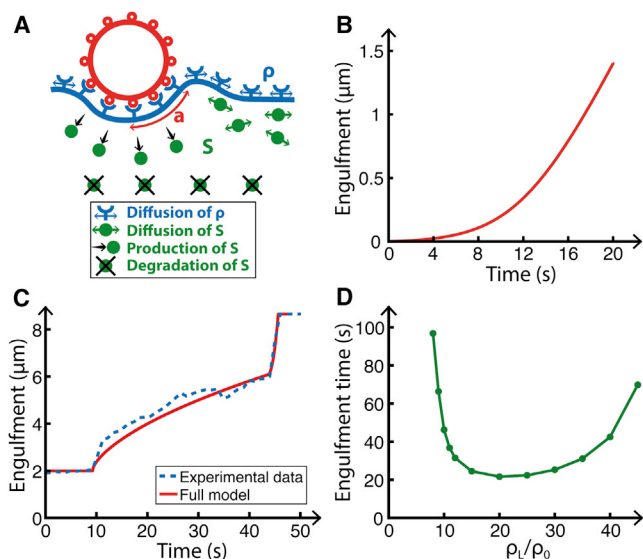
FIGURE 6 Engulfment model with signaling. (*A*) Sketch of the model which, in addition to the receptor density ρ, contains a signaling molecule with density S. Receptors can only diffuse (with diffusion constant D) and drift (with speed v), whereas the signaling molecule is produced within the cup with rate $\beta\rho_L$, degraded everywhere with lifetime τ, and diffuses with diffusion constant D_S. (*B*) In contrast to other models, the rate of engulfment can now accelerate if the drift velocity depends linearly on S via $v = v_1 S$, tending to a constant as $t \to \infty$. Parameters are $v_1 = 20\ \mu m^3$ s^{-1}, $\beta = 0.1\ s^{-1}$, $\tau = 10$ s, and $R = 2\ \mu m$, no diffusion. (*C*) In the full model, with a drift velocity that depends on the signaling molecule via a threshold, S_0, and an initial latent period, t_0, a sharp increase in engulfment rate can be obtained, which matches well with the measured data. Here the measured data is the average of the upper and lower lobes for the 4.6-μm bead shown in Fig. 2 *C*. Parameters are $D = 3.8\ \mu m^2\ s^{-1}$, $v_1 = 6\ \mu m^3\ s^{-1}$, $S_0 = 0.498$ μm^{-2}, $\beta = 0.4\ s^{-1}$, $\tau = 0.5$ s, $t_0 = 10$ s, and $R = 2.75\ \mu m$. (*D*) The dependence of the full-engulfment time on the ligand density, ρ_L, showing a minimum at intermediate ρ_L. Parameters as in panel *C*. Additional parameters are $\rho_0 = 50\ \mu m^{-2}$, $\mathscr{E} = 3$, $\mathscr{B} = 20$, $D_S = 1\ \mu m^2\ s^{-1}$, and $L = 50\ \mu m$. To see this figure in color, go online.

increases, the drift velocity also increases, leading to quicker and quicker engulfment.

The effect of signaling on the drift velocity is likely to be cooperative, with multiple signaling molecules required to activate drift. Although we could model this via Hill-like behavior with a large Hill coefficient, we instead choose, for simplicity, to use a threshold S_0. Receptors diffuse until the signaling molecule at the cup edge reaches S_0. At this point, constant drift is turned on at all positions. This model, as shown in Fig. 6 *C*, contains a rapid increase in the rate of engulfment when S_+ reaches S_0.

To complete our model we introduce an initial latent period of length t_0, representing the period when the particle sits on the cell, before engulfment begins. By fitting the model parameters, we obtain good agreement with our experimental data. For example, Fig. 6 *C* shows the fit with the data from the 4.6-μm bead shown in Fig. 2 *C* (averaged over the upper and lower lobes). Although simple, our model correctly captures the main features we observed dur-

ing engulfment, including the two-stage behavior of the cup edge.

How engulfment depends on the ligand density

Using our full model, we now study the dependence of the engulfment time on the ligand density, ρ_L. This is not trivial because ρ_L appears in the cup growth rate (Eq. 2b), the receptor density at the cup edge (Eq. 4), and the production rate of the signaling molecule (Eq. 9). From our simulations we measure the full-engulfment time for various ρ_L (Fig. 6 *D*).

Interestingly, the behavior is not monotonic. For small ligand densities, the signaling molecule production rate is small and S only slowly increases toward S_0, leading to a long engulfment time. As ρ_L increases, this production rate increases, which tends to reduce the engulfment time. However, at the same time, the cup growth rate decreases (because more ligands must be bound), so that the region of S production ($r < a$) is smaller. This has the tendency to increase the engulfment time. These two competing effects lead to the nonmonotonic behavior, with an initial decrease before a final rise as ρ_L is increased. Notably, this predicts an optimum intermediate ligand density corresponding to the quickest possible engulfment. This is in sharp contrast to previous models (such as Gao et al. (18) and Decuzzi and Ferrari (30)), where the engulfment time monotonically increases with increasing ligand density (see Fig. S3 *E*). However, such models do not include signaling and neglect the two-stage nature of engulfment.

Although some previous experimental work has addressed the dependence of phagocytosis on ligand density (31,32), this usually involved measuring the percentage of engulfed particles, rather than the progression of the cup with time. This is more a measure of how often engulfment stalls, and is unlikely to be directly related to the engulfment rate. The engulfment time was measured in Zhang et al. (31), with similar cup closure times at different ρ_L. However, because only two ligand densities were studied, this does not conflict with our prediction, for which ligand densities either side of the optimum density can have similar engulfment times.

Ellipsoidal particles engulf quickest when presented tip-first

Finally, we study the effect of nonspherical particles. Because we are considering a one-dimensional model, our particles must be rotationally symmetric. For simplicity, we only consider spheroids—that is, ellipsoids where two of the principal axes have identical lengths. Thus spheroids are described by two parameters: R_1, the radius parallel to the membrane, and R_2, the radius perpendicular to the membrane (Fig. 7 *A*). The only difference from the above model is that κ_p in Eq. 4 is now $2H$, where H is the mean curvature
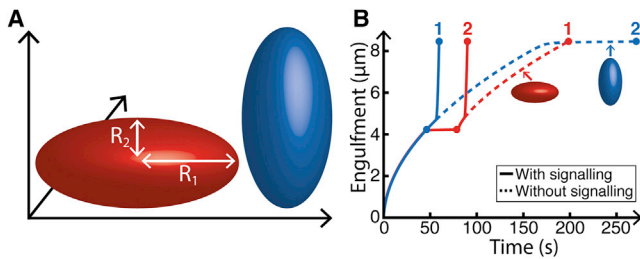
FIGURE 7 Comparison of oblate and prolate spheroids. (A) Sketch of the two spheroids, parameterized by R_1 and R_2. For oblate spheroids ($R_1 > R_2$), the lowest curvature region is the first to be engulfed, whereas for prolate spheroids ($R_1 < R_2$), the highest curvature region is engulfed first. (B) Progression of engulfment with time. (Red) Oblate spheroid with $R_1 = R_2 = 4.1$ μm and $R_3 = 0.62$ μm. (Blue) Prolate spheroid with $R_1 = R_2 = 0.87$ μm and $R_3 = 4$ μm. (Solid lines) Full model with signaling; (dashed lines) pure diffusion model without signaling. (Solid circles) Half- and full engulfment. (Numbers) Order of engulfment. To see this figure in color, go online.

of the spheroid. By using the standard parameterization of the surface of a spheroid,

$$
\begin{aligned}
x &= R_1 \sin v \cos u, \\
y &= R_1 \sin v \sin u, \\
z &= -R_2 \cos v,
\end{aligned}
\tag{10}
$$

where $u \in [0, 2\pi)$ and $v \in [0, \pi]$, we can write the mean curvature as (33)

$$
2H = \frac{R_2 \left[R_1^2 (1 + \cos^2 v) + R_2^2 \sin^2 v \right]}{R_1 \left(R_1^2 \cos^2 v + R_2^2 \sin^2 v \right)^{3/2}}.
\tag{11}
$$

At any given time, we determine the value of v at the cup edge (corresponding to engulfed arc length a) and hence the curvature at $r = a$. This, via Eq. 4, gives the value of the receptor density at the cup edge, ρ_+. High curvature regions lead to relatively large values of ρ_+, and hence to slower engulfment.

Because we can only consider particles with two equal axes, we cannot directly compare the standing and lying-down versions of the same spheroid. Instead, we compare a spheroid where $R_1 > R_2$ (which is an oblate spheroid as in the first shape in Fig. 7 A) with a spheroid with $R_1 < R_2$ (which is a prolate spheroid as in the second shape in Fig. 7 A). To make the comparison meaningful, we ensure that both spheroids have the same circumference (i.e., the same total engulfment length). We also assume that these high-symmetry orientations are stable during engulfment.

To begin, we study the (unnatural) situation with signaling turned off, i.e., our pure diffusion model. For the oblate spheroid, the curvature is initially low, increasing to a maximum at half-engulfment, before decreasing back to its initial value. This leads to a fast-slow-fast type of engulfment, with the slowest cup progression occurring near half-engulfment (red dashed curve in Fig. 7 B). In contrast, for the prolate spheroid, the highest curvatures occur at the beginning and end of engulfment. In principle, this leads

to slow-fast-slow engulfment, although the first stage is so short that it is better described as fast-slow engulfment (blue dashed curve in Fig. 7 B). Because the highest curvature region occurs toward the end in the prolate case, when the engulfment rate is already low, this has a much greater effect on cup progression, meaning that (without signaling) the prolate spheroid takes longer to engulf.

The situation, however, is markedly different for our full model with signaling (solid curves in Fig. 7 B). Although the prolate spheroid takes longer than the oblate spheroid to reach full engulfment, it reaches half-engulfment earlier. Consequently, the signaling molecule also reaches the threshold S_0 earlier, so that the second rapid engulfment stage begins sooner. Thus, with signaling, it is actually the prolate spheroid that is the first to complete engulfment. This agrees well with previous experimental observations, where nonspherical particles were found to be much easier to engulf when presented tip-first (34). A similar effect was observed in van Zon et al. (16), but in a model that ignores the two distinct stages of engulfment.

DISCUSSION

By analyzing time-lapse movies of neutrophils exposed to IgG-coated beads, we found evidence of two distinct stages during phagocytosis engulfment. The first stage proceeds relatively slowly, taking, on average, three-quarters of the total engulfment time to reach only half-engulfment. In contrast, engulfment is much quicker in the second stage, often only taking a few seconds. This is perhaps opposite to the expected behavior: the initial availability of spare membrane within membrane wrinkles might be thought to lead to quick initial engulfment, with a subsequent slowing as new membrane must be created or brought from internal stores (19,20). However, this argument can be turned on its head: perhaps it is precisely the need to create new membrane at approximately half-engulfment that is the signal for the cell to enter a second, more active phase of engulfment, with a rapid increase in engulfment speed.

This experimental observation seems to conflict with the result in Masters et al. (19), which also found two stages, but with an initial rapid stage followed by a slower second stage. However, Masters et al. (19) mostly involves macrophages spreading on a flat glass surface, whereas we study neutrophils engulfing spherical beads. This is likely to be substantially different both because of the huge difference in curvature (engulfment is highly dependent on curvature (18,34)) and, perhaps more importantly, because Masters et al. (19) necessarily involves frustrated phagocytosis, where engulfment can never complete. However, we believe the main difference occurs due to their large initial contact area, where cells placed on a glass surface instantly spread so that their initial contact area is ~140 μm^2 (see their Fig. 1 B), which is well above the total surface area for even our large 6.2-μm bead. Thus the

cells in Masters et al. (19) start with a contact area larger than that of complete engulfment for our beads, so that it seems likely that they may miss our initial slow stage when the cell is engulfing the first half of the target. Given this, the first stage in Masters et al. (19) should be identified with our second stage. It is perhaps also relevant that Masters et al. (19) used macrophages rather than neutrophils.

Motivated by the appearance of two stages, we then developed various models to describe engulfment. A complete mathematical model of phagocytosis is made difficult by the sheer number of parameters involved, which would in turn severely reduce its predictive power. Instead, we made progress by considering simplified models that only focus on the key components, ignoring the role of myosins, the need for cytoskeletal remodeling, and the full three-dimensional membrane shape. Motivated by the elegant model of endocytosis in Gao et al. (18), our simplest model only focused on the Fcγ receptors and assumed that the membrane appeared flat to the receptors. Although these are significant simplifications, we believe that our model still gives useful information about how the cell organizes phagocytosis and can correctly capture the basic receptor dynamics. By the addition of receptor drift and a signaling molecule, we were able to develop a full, yet still simple, model that captures the sharp jump in engulfment rate.

The switch to the second stage occurs, on average, at almost exactly half-engulfment, which is precisely the point when the cell must start to tighten the cup around the top-half of the particle for cup closure. This switch could provide an alternative explanation to the observation in van Zon et al. (16) that cells either fully engulf a target particle or stall before the half-way point. If, sometimes, perhaps due to insufficient signaling, the trigger for the second stage does not occur, this would leave cells at half-engulfment, without the necessary new membrane or modified receptor dynamics to enter the second stage and proceed to full engulfment.

How could the cell identify and signal the switch to the second stage of engulfment? Identification could be achieved in a variety of ways, perhaps by the increased membrane tension during engulfment (19), by the exhaustion of membrane wrinkles (20), or by the reduced speed of engulfment. With regard to signaling, various proteins are known to be expressed at later stages of engulfment and may therefore serve as the signal for the switch (3,31,35). For example, Rac1 and Rac2 (small signaling GTPases) localize to the cup well after engulfment begins, with Rac1 appearing first (36). Similarly, PKCε, a serine/threonine kinase, is only involved during the later stages of cup formation (37). Although originally thought to be important only when the phagosome is fully formed, it was shown in Zhang et al. (31) that PKCε reaches one-half its maximum signal well before cup closure. Because stalled cups do not recruit PKCε (31), this would also

tally with PKCε playing some role during the second stage of engulfment. Finally, phosphatidylinositol 3-kinase has been shown to be required for phagosome contraction during the later stages of engulfment (38).

The second stage is markedly faster than the first. With engulfment described by a power law, $a \sim At^\alpha$, this increased engulfment rate could be achieved either by increasing the prefactor A, increasing the power α, or by a combination of both. Our fit to the data (and our full model) suggests an increase in the power ($\alpha_2 \gtrsim 1$), corresponding to the activation of drift in response to signaling (Fig. 6). Such active drift motion of receptors toward the cup could be achieved, for example, by coupling the receptors to centripetal actin dynamics as observed in immunological synapses (29). In addition, it is likely that actin plays a role during the second stage, perhaps mediated by myosin IC (28). The full model leads to an interesting prediction for the receptor density near the cup. As seen in Fig. 5, A and B, the switch from diffusion to drift causes the sign of the receptor density gradient to switch immediately outside the cup: the depletion seen near the cup in the first stage disappears during the second stage. It would be interesting to tag the Fcγ receptor and try to observe this. Further, and perhaps surprisingly, our model predicts that the quickest engulfment occurs for some intermediate value of the ligand density, a claim that would also be interesting to test. In addition, we found that our model can explain the observation that tip-first ellipsoids are easier to engulf. In fact, our model goes further and predicts the entire engulfment time course for such particles, a result that could also be tested, perhaps with the same micropipette assay used in Herant et al. (14).

Although our analysis favors an increase in the power α during the second stage, it is also possible that the cell implements the faster engulfment stage by increasing the prefactor A. This would still require active processes, but now the second stage would correspond to the pure diffusion model (as with the first stage), but with altered parameters. As explained in the Supporting Material, such behavior could be achieved either by increasing the receptor diffusion constant D, increasing the receptor-ligand binding strength $\mathscr{E}$, decreasing the bending strength $\mathscr{B}$, or by increasing the total number of receptors. Biologically these parameter changes could potentially be achieved by posttranslational modifications of the receptors, by receptor clustering (39), or by modifying the membrane structure (perhaps by altering lipid composition (40) or the connection with the actin cytoskeleton (41)). Models where the prefactor A increases would differ from those where the power α increases, because the receptor density would remain depleted just outside the cup even during the second stage. Thus, in principle, fluorescence microscopy of tagged receptors could distinguish between these two scenarios.

Understanding phagocytosis is of vital importance, given its crucial role in the immune system and its relevance to drug delivery (42). Despite the staggering molecular

complexity, simple physical mechanisms constrain and simplify the process, including membrane capacity (43), particle stiffness (44), and particle shape (34). Our simplified mathematical model shows that cells employ a multistage approach to engulfment, with radically different receptor dynamics occurring during different stages of engulfment. Potentially the second stage is a later evolutionary addition, resulting in increased engulfment speed and robustness. Conversely, such an approach may help overcome the difficulty of engulfing the final part of the target, or perhaps function as a means of first examining the particle, a way of checking the desirability and feasibility of engulfment, before fully committing the cell machinery to the engulfment process.

SUPPORTING MATERIAL

SUPPORTING CITATIONS

References (45–51) appear in the Supporting Material.

REFERENCES

1. Flannagan, R. S., V. Jaumouillé, and S. Grinstein. 2012. The cell biology of phagocytosis. *Annu. Rev. Pathol.* 7:61–98.

2. Botelho, R. J., and S. Grinstein. 2011. Phagocytosis. *Curr. Biol.* 21:R533–R538.

3. Swanson, J. A. 2008. Shaping cups into phagosomes and macropinosomes. *Nat. Rev. Mol. Cell Biol.* 9:639–649.

4. Griffin, Jr., F. M., J. A. Griffin, …, S. C. Silverstein. 1975. Studies on the mechanism of phagocytosis. I. Requirements for circumferential attachment of particle-bound ligands to specific receptors on the macrophage plasma membrane. *J. Exp. Med.* 142:1263–1282.

5. Griffin, Jr., F. M., J. A. Griffin, and S. C. Silverstein. 1976. Studies on the mechanism of phagocytosis. II. The interaction of macrophages with anti-immunoglobulin IgG-coated bone marrow-derived lymphocytes. *J. Exp. Med.* 144:788–809.

6. McKenzie, S. E., and A. D. Schreiber. 1998. Fcγ receptors in phagocytes. *Curr. Opin. Hematol.* 5:16–21.

7. Joshi, T., J. P. Butchar, and S. Tridandapani. 2006. Fcγ receptor signaling in phagocytes. *Int. J. Hematol.* 84:210–216.

8. Nimmerjahn, F., and J. V. Ravetch. 2008. Fcγ receptors as regulators of immune responses. *Nat. Rev. Immunol.* 8:34–47.

9. Berton, G., A. Mócsai, and C. A. Lowell. 2005. Src and Syk kinases: key regulators of phagocytic cell activation. *Trends Immunol.* 26:208–214.

10. Diakonova, M., G. Bokoch, and J. A. Swanson. 2002. Dynamics of cytoskeletal proteins during Fcγ receptor-mediated phagocytosis in macrophages. *Mol. Biol. Cell.* 13:402–411.

11. Dart, A. E., S. Tollis, …, R. G. Endres. 2012. The motor protein myosin 1G functions in FcγR-mediated phagocytosis. *J. Cell Sci.* 125:6020–6029.

12. Underhill, D. M., and A. Ozinsky. 2002. Phagocytosis of microbes: complexity in action. *Annu. Rev. Immunol.* 20:825–852.

13. Metchnikoff, É. 1884. About anthrax bacilli on the relationship of phagocytes [Über die Beziehung der Phagocyten zu Milzbrandbacillen]. *Arch. Pathol. Anat.* 97:502–526.

14. Herant, M., V. Heinrich, and M. Dembo. 2006. Mechanics of neutrophil phagocytosis: experiments and quantitative models. *J. Cell Sci.* 119:1903–1913.

15. Herant, M., C.-Y. Lee, …, V. Heinrich. 2011. Protrusive push versus enveloping embrace: computational model of phagocytosis predicts key regulatory role of cytoskeletal membrane anchors. *PLOS Comput. Biol.* 7:e1001068.

16. van Zon, J. S., G. Tzircotis, …, M. Howard. 2009. A mechanical bottleneck explains the variation in cup growth during FcγR phagocytosis. *Mol. Syst. Biol.* 5:298.

17. Tollis, S., A. E. Dart, …, R. G. Endres. 2010. The zipper mechanism in phagocytosis: energetic requirements and variability in phagocytic cup shape. *BMC Syst. Biol.* 4:149.

18. Gao, H., W. Shi, and L. B. Freund. 2005. Mechanics of receptor-mediated endocytosis. *Proc. Natl. Acad. Sci. USA.* 102:9469–9474.

19. Masters, T. A., B. Pontes, …, N. C. Gauthier. 2013. Plasma membrane tension orchestrates membrane trafficking, cytoskeletal remodeling, and biochemical signaling during phagocytosis. *Proc. Natl. Acad. Sci. USA.* 110:11875–11880.

20. Hallett, M. B., and S. Dewitt. 2007. Ironing out the wrinkles of neutrophil phagocytosis. *Trends Cell Biol.* 17:209–214.

21. Lee, C. Y., M. Herant, and V. Heinrich. 2011. Target-specific mechanics of phagocytosis: protrusive neutrophil response to zymosan differs from the uptake of antibody-tagged pathogens. *J. Cell Sci.* 124:1106–1114.

22. Heinrich, V., and W. Rawicz. 2005. Automated, high-resolution micropipet aspiration reveals new insight into the physical properties of fluid membranes. *Langmuir.* 21:1962–1971.

23. Herant, M., V. Heinrich, and M. Dembo. 2005. Mechanics of neutrophil phagocytosis: behavior of the cortical tension. *J. Cell Sci.* 118:1789–1797.

24. Quinn, P., G. Griffiths, and G. Warren. 1984. Density of newly synthesized plasma membrane proteins in intracellular membranes II. Biochemical studies. *J. Cell Biol.* 98:2142–2147.

25. Gandour, D. M., and W. S. Walker. 1983. Macrophage cell cycling: influence on Fc receptors and antibody-dependent phagocytosis. *J. Immunol.* 130:1108–1112.

26. Raychaudhuri, G., D. McCool, and R. H. Painter. 1985. Human IgG1 and its Fc fragment bind with different affinities to the Fc receptors on the human U937, HL-60 and ML-1 cell lines. *Mol. Immunol.* 22:1009–1019.

27. Pontes, B., Y. Ayala, …, H. M. Nussenzveig. 2013. Membrane elastic properties and cell function. *PLoS ONE.* 8:e67708.

28. Swanson, J. A., M. T. Johnson, …, N. Araki. 1999. A contractile activity that closes phagosomes in macrophages. *J. Cell Sci.* 112:307–316.

29. Yu, C. H., H.-J. Wu, …, J. T. Groves. 2010. Altered actin centripetal retrograde flow in physically restricted immunological synapses. *PLoS ONE.* 5:e11878.

30. Decuzzi, P., and M. Ferrari. 2007. The role of specific and non-specific interactions in receptor-mediated endocytosis of nanoparticles. *Biomaterials.* 28:2915–2922.

31. Zhang, Y., A. D. Hoppe, and J. A. Swanson. 2010. Coordination of Fc receptor signaling regulates cellular commitment to phagocytosis. *Proc. Natl. Acad. Sci. USA.* 107:19332–19337.

32. Pacheco, P., D. White, and T. Sulchek. 2013. Effects of microparticle size and Fc density on macrophage phagocytosis. *PLoS ONE.* 8:e60989.

33. Weisstein, E. W. 2014. Ellipsoid. *MathWorld—A Wolfram Web Resource*. http://mathworld.wolfram.com/Ellipsoid.html. Accessed May 28, 2014.

34. Champion, J. A., and S. Mitragotri. 2006. Role of target geometry in phagocytosis. *Proc. Natl. Acad. Sci. USA*. 103:4930–4934.

35. Swanson, J. A., and A. D. Hoppe. 2004. The coordination of signaling during Fc receptor-mediated phagocytosis. *J. Leukoc. Biol.* 76:1093–1103.

36. Hoppe, A. D., and J. A. Swanson. 2004. Cdc42, Rac1, and Rac2 display distinct patterns of activation during phagocytosis. *Mol. Biol. Cell.* 15:3509–3519.

37. Larsen, E. C., T. Ueyama, …, M. R. Lennartz. 2002. A role for PKC-ε in FcγR-mediated phagocytosis by RAW 264.7 cells. *J. Cell Biol.* 159:939–944.

38. Araki, N., M. T. Johnson, and J. A. Swanson. 1996. A role for phosphoinositide 3-kinase in the completion of macropinocytosis and phagocytosis by macrophages. *J. Cell Biol.* 135:1249–1260.

39. Sobota, A., A. Strzelecka-Kiliszek, …, K. Kwiatkowska. 2005. Binding of IgG-opsonized particles to Fcγ R is an active stage of phagocytosis that involves receptor clustering and phosphorylation. *J. Immunol.* 175:4450–4457.

40. Mercanti, V., S. J. Charette, …, P. Cosson. 2006. Selective membrane exclusion in phagocytic and macropinocytic cups. *J. Cell Sci.* 119:4079–4087.

41. Andrews, N. L., K. A. Lidke, …, D. S. Lidke. 2008. Actin restricts FcεRI diffusion and facilitates antigen-induced receptor immobilization. *Nat. Cell Biol.* 10:955–963.

42. Lin, S.-Y., W.-H. Hsu, …, G.-H. Hsiue. 2011. Novel geometry type of nanocarriers mitigated the phagocytosis for drug delivery. *J. Control. Release.* 154:84–92.

43. Cannon, G. J., and J. A. Swanson. 1992. The macrophage capacity for phagocytosis. *J. Cell Sci.* 101:907–913.

44. Beningo, K. A., and Y. L. Wang. 2002. Fc-receptor-mediated phagocytosis is regulated by mechanical properties of the target. *J. Cell Sci.* 115:849–856.

45. Gonzalez, R., and R. Woods. 2007. Digital Image Processing. Prentice Hall, Upper Saddle River, NJ, pp. 728–736.

46. Duda, R. O., and P. E. Hart. 1972. Use of the Hough transformation to detect lines and curves in pictures. *Commun. ACM.* 15:11–15.

47. Helfrich, W. 1973. Elastic properties of lipid bilayers: theory and possible experiments. *Z. Naturforsch. C.* 28:693–703.

48. Freund, L. B., and Y. Lin. 2004. The role of binder mobility in spontaneous adhesive contact and implications for cell adhesion. *J. Mech. Phys. Solids.* 52:2455–2472.

49. Myers, T. G., S. L. Mitchell, and F. Font. 2012. Energy conservation in the one-phase supercooled Stefan problem. *Int. Commun. Heat Mass.* 39:1522–1525.

50. Chadam, J., and P. Ortoleva. 1983. The stability effect of surface tension on the development of the free boundary in a planar, one-dimensional, Cauchy-Stefan problem. *IMA J. Appl. Math.* 30:57–66.

51. Dewynne, J. N., S. D. Howison, …, W. Xie. 1989. Asymptotic behavior of solutions to the Stefan problem with a kinetic condition at the free boundary. *J. Austral. Math. Soc. Ser. B.* 31:81–96.